



Chen Huizheng · Zhong Shun  · Lu Zhenyong ·  
Chen Yushu · Han Jiajie · Wang Chao

# Analysis on multi-mode nonlinear resonance and jump behavior of an asymmetric rolling bearing rotor

Received: 27 October 2020 / Accepted: 24 March 2021 / Published online: 2 April 2021  
© The Author(s), under exclusive licence to Springer-Verlag GmbH Germany, part of Springer Nature 2021

**Abstract** This paper takes an asymmetric support ball bearing-rotor system subjected by unbalanced force and parametric excitation (varying compliance) as the research object. Multi-modes of resonance such as natural frequency resonance region of each order, VC (varying compliance) frequency resonance region, the 1/2 sub-harmonic VC frequency resonance region, and quasi-periodic regions, and the nonlinear characteristics in these regions are analyzed. Besides, the effect of the number of balls of the ball bearing is also considered and the result shows that the parity of this parameter matters a lot. By introducing a definition of the absolute quasi-periodic frequency, the law of the occurrence of the quasi-periodic motion is demonstrated and the possible cause is given to some extent. The work provides a theoretical basis for clarifying the nonlinear characteristics of the bearing-rotor system and suppressing the nonlinear behavior of the system.

**Keywords** Rolling element bearing · Asymmetric support · Jeffcott rotor · Frequency–amplitude response · VC frequency resonance · Quasi-periodic response

## 1 Introduction

Rolling element bearings are a type of main support for rotating machinery, especially for the rotors of aero-engines, and are a key source of vibration (parametric excitation) in rotor-bearing systems, which create a demand for vibration analysis and diagnostic techniques under various operating conditions. Mainly including the inner and outer rings, cages and balls or rollers, the complicated mechanical structure of a rolling element bearing exhibits nonlinear behavior due to bearing clearance, nonlinear Hertzian contact force, and defects. With the presence of rotating unbalance, which is unavoidable, a wide variety of nonlinear behaviors can be expected. These would add difficulties and obstacles to system status determination, prediction and control. Therefore, studying the nonlinear behavior of the system and identifying the influence of rolling element bearing parameters on the nonlinear behaviors of the rotor system will help to reasonably avoid system instability, increase the operating life, and improve the efficiency of mechanical equipment.

For a vibrating system, when the external excitation frequency is equal to the natural frequency of each order of the system, the main resonances of each order occur. But nonlinearities in the system lead linear

---

C. Huizheng · L. Zhenyong  
Institute of Dynamics and Control Science, Shandong Normal University, Jinan 250014, China

Z. Shun (✉) · C. Yushu  
Department of Mechanics and Key Laboratory of Nonlinear Dynamics and Control, Tianjin University, Tianjin 300072, China  
Z. Shun  
E-mail: shunzhong@tju.edu.cn

H. Jiajie · W. Chao  
Hebei Ruizhao Laser Remanufacturing Technology Stock Co., Ltd, Tangshan 064300, China

resonance changing to nonlinear resonance, which is more complicated and wider in range. To a ball bearing rotor, the nonlinearities introduced by the clearance and the contact force between the rollers and rings and the unavoidable rotor unbalance make the rolling element bearing-rotor system a complex nonlinear system. Using nonlinear models, the vibration analysis of rotor-bearing systems has received considerable attention. The early research of the nonlinear phenomena in rolling element bearings can be traced back to 80s. Fukuta et al. [1] found that ball bearing systems have nonlinear dynamic behaviors such as super-harmonic, sub-harmonic, quasi-periodic, and chaos-like solutions. Mevel and Guyader [2,3] studied the path of the bearing system entering chaos through theory and experiments. He pointed out that the system had a way to enter chaos through the period-doubling bifurcation and quasi-period path, and explained the relationship between chaos motion and the contact failure (loss contact).

For the effects of the clearance, Saito [4] found that there are hard spring characteristics and soft spring characteristics in different vibration modes in a bearing-rotor system with clearance. Feng and Hahn [5] experimentally studied the effects of clearance on bearing dynamics and confirmed the existence of multiple solutions. Tiwari et al. [6,7] changed stiffness and unbalanced excitation frequency together. By increasing the clearance and increasing the variable compliance frequencies of super-harmonic and sub-harmonic responses, the flexible rotor had intermittent chaos. The stability analysis of the bearing-supported unbalanced rotor system was carried out. It was found that the system had three high-amplitude regions, which are, respectively, the period-doubling bifurcation caused by instability of the period-1 solution and the quasi-period solution due to the Hopf bifurcation and  $1/2$  VC frequency. Bai et al. [8] studied the effects of bearing clearance on the stability of the system. In addition to the norm form of instability via period-doubling bifurcation and secondary Hopf bifurcation, there is also a boundary crisis bifurcation. When the rotating speed exceeded the critical value, the chaotic attractor appeared suddenly. Kostek [9] studied the effects of bearing clearance changes on the dynamic behaviors of the system. As the clearance increased, typical nonlinear phenomena such as bi-stable state, chaotic motion, period window, and period-doubling bifurcation appeared in the system. They were very sensitive to the changes of the clearance.

Besides the nonlinear behaviors introduced by the clearance, Harsha [10,11] considered the Hertzian contact force, waviness, clearance, and other factors of rolling bearings to obtain nonlinear characteristics such as sub-harmonic, quasi-periodic motion, and chaotic motion in the bearing-rotor system. Guputa et al. [12] found chaos when the VC frequency of the flexible rotor approached the first natural frequency of the system. Jin et al. [13] verified the coexistence of soft and hard stiffness characteristics of system resonance peaks caused by bearing contact resonance through experiments.

Moreover, Jump phenomena were observed during the run-up and run-down with the constant operation. Villa et al. [14] performed a stability analysis on a flexible rotor supported by a rolling element bearing, and found that there were two jump intervals in the range of the first-order main resonance region, and pointed out that the contact between the rolling element and the outer ring of the bearing can be as many as three or even four in a period. Maraini and Nataraj [15] found that bearing clearance caused the system resonance peak to exhibit the characteristics of hard spring, and external load force caused the system resonance peak to exhibit the characteristic of soft spring, and both could induce jump phenomenon.

Several researchers have studied the rotor-bearing system using a nonlinear analysis technique known as the harmonic balance method. Yang et al. [16] employed harmonic balance method to solve the dynamic equations of cracked uncertain hollow-shaft system. Sinou [17] used the harmonic balance method to analyze the system and found that the frequencies 2, 3, and 6 in the system dominated, and the super-harmonic and sub-harmonic of the corresponding frequency were generated. The change of the unbalance in the system would make the responses change from soft-hard spring characteristic to hard spring characteristic. Zhang et al. [18] integrated the harmonic balance method and pseudo-arc-length continuation method to analyze the hysteresis and bifurcation behavior of the bearing-balance rotor system, and revealed that the period-doubling bifurcation mechanism in the parametric resonance region is 1:2 internal resonance.

Most of these previous studies utilized numerical integration techniques and analytical methods such as the harmonic balance method. Some nonlinear behaviors had been discovered, but more are expected, especially in the region of jump where multiple solutions exist. Thus, in this paper, we will focus on the nonlinear behaviors especial for the jump resonance phenomenon of a Jeffcott rotor-bearing system with clearance and nonlinear Hertzian contact using a mathematical representation with fractional power. Using the derived describing function for the bearing force, the frequency responses can be got by numerical means further. Meanwhile, based on the work by Harsha et al. [19] and Aktürk et al. [20], we know that the number of balls has huge effect on the nonlinear behaviors of the ball bearing-rotor system, thus in this paper the effects of the number of balls will be discussed in detail. Meanwhile, in the current researches on bearing-rotor systems, there are more

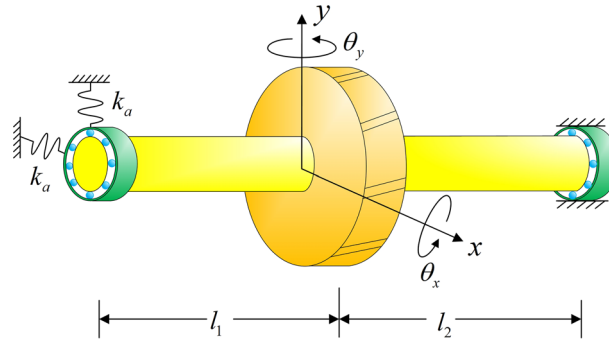


Fig. 1 Schematic diagram of a Jeffcott rotor with ball bearings

studies on bearing parametric resonance or main resonance. Quasi-periodic behavior research is relatively less. Considering the asymmetry of mass and stiffness, this work will take a rotor system supported by rolling bearings as a model and try to find out the occurrence rule of the quasi-periodic motion.

The goal of this work is to find the nonlinear resonance phenomena introduced by nonlinearities of rolling element bearing in as many as possible frequency regions and find out the possible reasonable reason of the formation. A secondary objective is to provide a better understanding of bearing behaviors by studying the frequency response and effects of the parameters, such as number of balls, on the system. The specific content of the work is organized as follows: a brief introduction has been given in Sect. 1. In Sect. 2, the governing equations of an asymmetric support Jeffcott rotor will be established. Then based on the model get in Sect. 2, the resonance phenomena and parameter discussion in the main resonance region, VC frequency resonance region, the 1/2 sub-harmonic VC frequency resonance region, and some quasi-periodic resonance regions will be studied step by step. Concluding remarks will be given finally.

## 2 Modeling and foundation of dynamic equations

Figure 1 shows a schematic diagram of a rotor system supported by ball bearings. The left and right ends have different ball bearing support schemes, respectively, as the left end is connected to the foundation with a spring, and the right end is directly connected to the foundation. So the DOF (degree of freedom) of the outer ring of the left bearing should be considered while the right can be ignored.

Considering the gravity, unbalanced force, gyroscopic effect, and bearing force, the dynamic model of the rotor support structure shown in Fig. 1 can be established into form

$$\mathbf{M}\ddot{\mathbf{X}} + (\mathbf{C} + \Omega\mathbf{G})\dot{\mathbf{X}} + \mathbf{K}\mathbf{X} + \mathbf{F}_n = \mathbf{F}_u + \mathbf{F}_g \tag{1}$$

where  $\mathbf{X} = [\mathbf{x}, \mathbf{y}, \theta_x, \theta_y, x_a, y_a, x_b, y_b, x_o, y_o]^T$  is displacement coordinate vector, in which  $x$  and  $y$  are disk center's displacements along the  $x$ -axis and  $y$ -axis, respectively;  $\theta_x$  and  $\theta_y$  are disk center's rotation angles along the  $x$ -axis and  $y$ -axis, respectively;  $x_a$  and  $y_a$  represent the displacements of the equivalent mass at the left end;  $x_b$  and  $y_b$  represent the displacements of the equivalent mass at the right end; and,  $x_o$  and  $y_o$  represent the displacements of the outer ring of the bearing mounted at the left.  $\mathbf{M}$ ,  $\mathbf{C}$ ,  $\mathbf{G}$  and  $\mathbf{K}$  are corresponding mass matrix, damping matrix, gyro matrix and stiffness matrix.  $\mathbf{F}_n$  is the bearing force vector;  $\mathbf{F}_u$  is unbalanced force vector and  $\mathbf{F}_g$  is gravity vector.  $\Omega$  is rotating frequency which determines the frequency of the unbalanced force. The expanded form of Eq. (1) can be found in appendix.

The model has two supports, then the ball bearing force vector has form of

$$\mathbf{F}_n = [0, 0, 0, 0, F_{bx1}, F_{by1}, F_{bx2}, F_{by2}, -F_{bx1}, -F_{by1}]^T.$$

And the bearing force model adopted in this work is a two-degree-of-freedom ball bearing model, including nonlinear Hertzian contact force, clearance, and variable stiffness characteristics. Assuming that the initial positions of the bearing balls at both ends are the same, the position of the ball  $i$  at time  $t$  can be expressed as

$$\theta_i = 2\pi(i - 1)/N_b + \Omega_c t \tag{2}$$

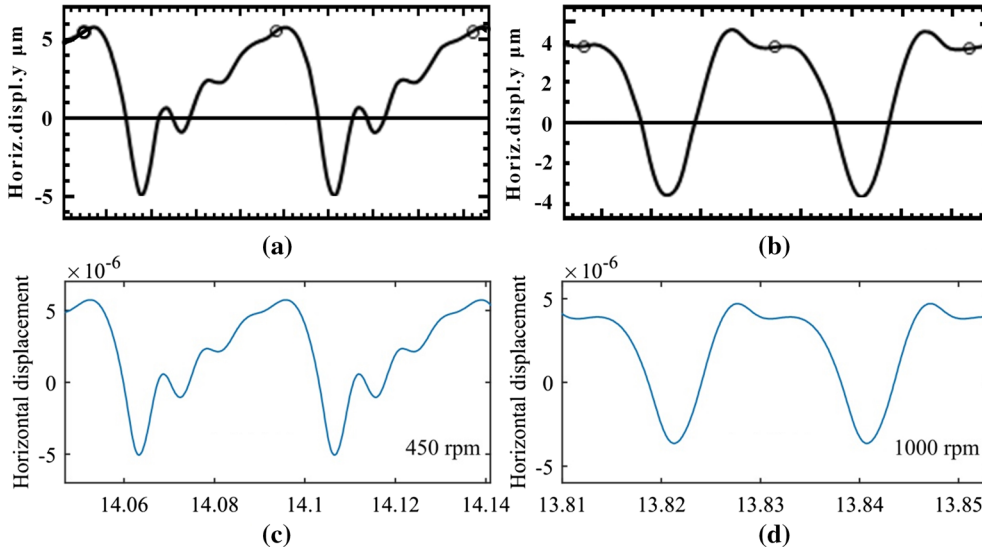


**Fig. 2** Comparisons of the bearing forces from [1] and calculated in this work: **a** Fukata’s result at 450 rpm; **b** Fukata’s result at 1000 rpm; **c** result from this work at 450 rpm; **d** result from this work at 1000 rpm

where  $N_b$  is the number of the rolling balls.  $\Omega_c = r_i / (r_i + r_o) \cdot \Omega$ , in which,  $r_i$  is the radius of the inner ring and  $r_o$  the radius of the outer ring.

Then, the bearing force of the left end can be expressed as Eq. (3)

$$\begin{bmatrix} F_{bx1} \\ F_{by1} \end{bmatrix} = C_b \sum_{i=1}^{N_b} (\delta_{1i} G [\delta_{1i}])^{3/2} \begin{bmatrix} \cos \theta_{1i} \\ \sin \theta_{1i} \end{bmatrix} \tag{3}$$

where  $\delta_{1i} = (x_a - x_o) \cos \theta_i + (y_a - y_o) \sin \theta_i - \delta_0$ ;  $C_b$  is the Hertz contact stiffness;  $G[\cdot]$  is Heaviside function and  $\delta_0$  is the radial clearance of bearing.

Meanwhile, the bearing force of the right end can be expressed as

$$\begin{bmatrix} F_{bx2} \\ F_{by2} \end{bmatrix} = C_b \sum_{i=1}^{N_b} (\delta_{2i} G [\delta_{2i}])^{3/2} \begin{bmatrix} \cos \theta_{2i} \\ \sin \theta_{2i} \end{bmatrix} \tag{4}$$

where  $\delta_{2i} = x_b \cos \theta_i + y_b \sin \theta_i - \delta_0$ .

Using the parameters in the Fukata’s paper [1], the comparison simulation results are shown in Fig. 2, with Fig. 2c which is calculated from Eqs. (3) and (4) compares with Fig. 2a which is from Ref. [1] at speed 450 rpm and Fig. 2d compares with Fig. 2b at 1000 rpm. The comparison results show that the bearing force model adopted here is reasonable.

Defining the dimensionless time as  $\tau = \Omega t$  and dimensionless displacement vector  $\mathbf{Q} = \mathbf{E}\mathbf{X}$ , in which  $\mathbf{E} = \frac{1}{c} \text{diag}(1, 1, l, l, 1, 1, 1, 1, 1, 1)$ , Eq. (1) can be transformed into

$$\mathbf{Q}'' + (\bar{\mathbf{C}} + \bar{\mathbf{G}})\mathbf{Q}' + \bar{\mathbf{K}}\mathbf{Q} + \bar{\mathbf{F}}_n = \bar{\mathbf{F}}_u + \bar{\mathbf{F}}_g \tag{5}$$

where  $\bar{\mathbf{C}} = \frac{1}{\Omega} \mathbf{E}\mathbf{M}^{-1}\mathbf{C}\mathbf{E}^{-1}$  is dimensionless damping matrix;  $\bar{\mathbf{G}} = \mathbf{E}\mathbf{M}^{-1}\mathbf{G}\mathbf{E}^{-1}$  is dimensionless gyro matrix;  $\bar{\mathbf{K}} = \frac{1}{\Omega^2} \mathbf{E}\mathbf{M}^{-1}\mathbf{K}\mathbf{E}^{-1}$  is dimensionless stiffness matrix;  $\bar{\mathbf{F}}_n = \frac{1}{\Omega^2} \mathbf{E}\mathbf{M}^{-1}\mathbf{F}_n$  is dimensionless bearing force vector;  $\bar{\mathbf{F}}_u = \frac{1}{\Omega^2} \mathbf{E}\mathbf{M}^{-1}\mathbf{F}_u$  is dimensionless unbalanced force vector and  $\bar{\mathbf{F}}_g = \frac{1}{\Omega^2} \mathbf{E}\mathbf{M}^{-1}\mathbf{F}_g$  is dimensionless gravity vector. The superscript prime denotes the derivative with respect of dimensionless time. The expanded form of Eq. (5) can be found in appendix.

Because the natural frequencies are related to the numbers of bearing ball, before to simulate the resonance regions, we calculate the first three order natural frequencies with different ball numbers. The results are shown

**Table 1** The critical speed under different numbers of the bearing balls

| Ball number | $\Omega_{1x}$ (rad/s) | $\Omega_{1y}$ (rad/s) | $\Omega_{2x}$ (rad/s) | $\Omega_{2y}$ (rad/s) | $\Omega_{3x}$ (rad/s) | $\Omega_{3y}$ (rad/s) |
|-------------|-----------------------|-----------------------|-----------------------|-----------------------|-----------------------|-----------------------|
| 8           | 281                   | 303                   | 822                   | 969                   | 1788                  | 1818                  |
| 9           | 286                   | 307                   | 854                   | 1001                  | 1795                  | 1826                  |
| 10          | 290                   | 310                   | 883                   | 1032                  | 1801                  | 1834                  |
| 11          | 292                   | 312                   | 889                   | 1058                  | 1802                  | 1842                  |
| 12          | 295                   | 315                   | 915                   | 1083                  | 1807                  | 1849                  |
| 13          | 298                   | 318                   | 936                   | 1107                  | 1812                  | 1857                  |

**Table 2** The values of the parameters

| Rotor parameters                        | Value                   | Bearing parameters | Value                                |
|---|-------------------------|--------------------|--------------------------------------|
| $m$                                     | 120 kg                  | $r_i$              | 39.6 mm                              |
| $m_a$                                   | 12 kg                   | $r_o$              | 70.4 mm                              |
| $m_b$                                   | 18 kg                   | $m_o$              | 0.965 kg                             |
| $k_{rr}$                                | $7.4 \times 10^7$ N/m   | $C_b$              | $1.0 \times 10^9$ N/m <sup>3/2</sup> |
| $k_{r\varphi}$ and $k_{\varphi\varphi}$ | $2.77 \times 10^7$ N/m  |                    |                                      |
| $k_{\varphi\varphi}$                    | $6.15 \times 10^7$ N/m  |                    |                                      |
| $k_a$                                   | $1.0 \times 10^7$ N/m   |                    |                                      |
| $c_1$                                   | 266 N·s/m               |                    |                                      |
| $c_2$ and $c_3$                         | 99.6 N·s/m              |                    |                                      |
| $c_4$                                   | 221 Ns/m                |                    |                                      |
| $l_1$                                   | 0.8 m                   |                    |                                      |
| $l_2$                                   | 1.25 m                  |                    |                                      |
| $J_d$                                   | 2.5 kg·m <sup>2</sup>   |                    |                                      |
| $J_p$                                   | 2.5 kg·m <sup>2</sup>   |                    |                                      |
| $\delta$                                | $1.67 \times 10^{-6}$ m |                    |                                      |

in Table 1. The values of the system parameters are listed in Table 2. It should be mentioned that as the stiffness is time varying, the mean of the response valves are used here as

$$\begin{aligned}
 k_{xx} &= \frac{1}{N} \sum_{i=1}^N \frac{\partial F_x}{\partial x}(i \Delta \tau) \\
 k_{yy} &= \frac{1}{N} \sum_{i=1}^N \frac{\partial F_y}{\partial y}(i \Delta \tau)
 \end{aligned}
 \tag{6}$$

where  $N = T/\Delta\tau$  is the number of discrete points.

It can be seen that, as the number of balls increases, the support stiffness of the system increases, then the natural frequency of each order slowly rises. Because the system is asymmetric, the natural frequency in the horizontal direction is lower than the natural frequency in the vertical direction. Based on the result, a dimensionless frequency  $\lambda = \Omega/\Omega_0$  (we choose  $\Omega_0 = 300$  rad/s as an integer near the natural frequency) is introduced for further analysis.

### 3 Analysis and discussion

#### 3.1 The primary frequency resonance region

When the external excitation’s frequency matches the natural frequency of the system, we say that the main resonance occurs in the general sense. To the rotor system established in the previous section, the amplitude-frequency curve around the first-order natural frequency of the system is shown in Fig. 3, which shows that the response curve (no matter what value of  $N_b$  is) appears a hard spring characteristic when the rotating speed increases and decreases in the resonance region, i.e., the response jumps downward and when the speed decrease, it jumps upward. This jump behavior is consistent with existing research [21].

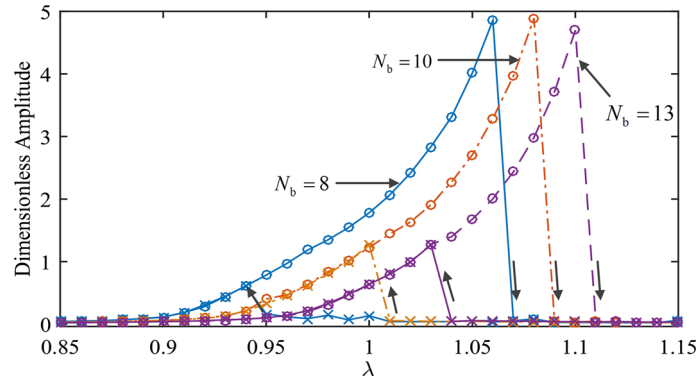


**Fig. 3** Amplitude-frequency curves in main resonance zone (where  $\circ$  indicates acceleration, and  $\times$  indicates deceleration)

Figure 3 also shows three curves in different colors as the number of the rolling balls varies, which could show us that when the number of the rolling balls increases, the equivalent stiffnesses of the system's supports increase, and the resonance peaks move to right without the hysteresis interval changing significantly. Compared with the two resonance cases studied in latter subsections, the resonance peak of the main resonance is much higher than the peak of the VC frequency resonance and its sub-harmonic resonance, so the magnitude of the main resonance amplitude determines the vibration level of the system as a whole.

There are many literature focused on the jump behaviors in the main resonance region. This work will not discuss it too much. But it is worth noting that for a nonlinear system, the super-harmonic or sub-harmonic response that may occur with the main resonance when the frequencies coincide, which will increase the amplitude of the response and further lead the resonance range wider. Also, the parametric characteristic of the bearing force will make the rotor system prone to instability.

### 3.2 The VC frequency resonance region

In ball bearing-rotor systems, in addition to the unbalanced excitation frequency, there are bearing VC frequencies related to the number of the balls. When the VC frequencies are equal to the system's natural frequencies, resonance behaviors also occur [22]. In this work, we call it VC frequency resonance.

Since the bearing VC frequency and the rotor unbalance excitation simultaneously present in the current system, each order critical speed of the system should correspond to at least two resonant regions: (1) the main resonance of the unbalanced excitation frequency and (2) the resonance of the bearing VC frequency.

Take  $N_b = 8$  as a research case, The first three orders of the equivalent natural frequencies of the system are converted into dimensionless parameters as  $\lambda_{1x} = 0.94$ ,  $\lambda_{1y} = 1.01$ ,  $\lambda_{2x} = 2.74$ ,  $\lambda_{2y} = 3.23$ ,  $\lambda_{3x} = 5.96$ , and  $\lambda_{3y} = 6.06$ . The dimensionless VC frequency can be calculated as  $\omega_{vc} = 2.88$  in this case. It can be determined that the system's VC frequency resonance points are  $\lambda_{v1x} = 0.326$  and  $\lambda_{v1y} = 0.351$ .

In order to prove the point of view in this work right, the amplitude-frequency characteristic curves in the horizontal and vertical directions when  $N_b = 8$  are used to be compared with Ref. [13]. The results are shown in Fig. 4.

Figure 4a, c shows the nonlinear behaviors in the horizontal direction through the VC frequency resonance region, and Fig. 4b, d shows the nonlinear behaviors in the vertical direction through the same region. It can be seen that in the horizontal direction, the system behaves as the amplitude jumps downward in both run-up and run-down process, which means it is a nonlinear characteristic of the coexistence of soft and hard stiffnesses, as in run-up process characteristics of a hard spring emerges while the characteristics of a soft spring in run-down process [22]. Unlike the horizontal direction, the vertical direction appears as a nonlinear characteristic of soft stiffness only.

Because the experimental conditions in Ref. [13] are complicated and there are additional factors such as horizontal additional stiffness and vertical additional load, it is difficult to quantitatively compare the results in this paper with the experimental results. But, the numerical analysis results well match the experiment results qualitatively, which could prove the validity of the analysis results in this paper to a certain extent.

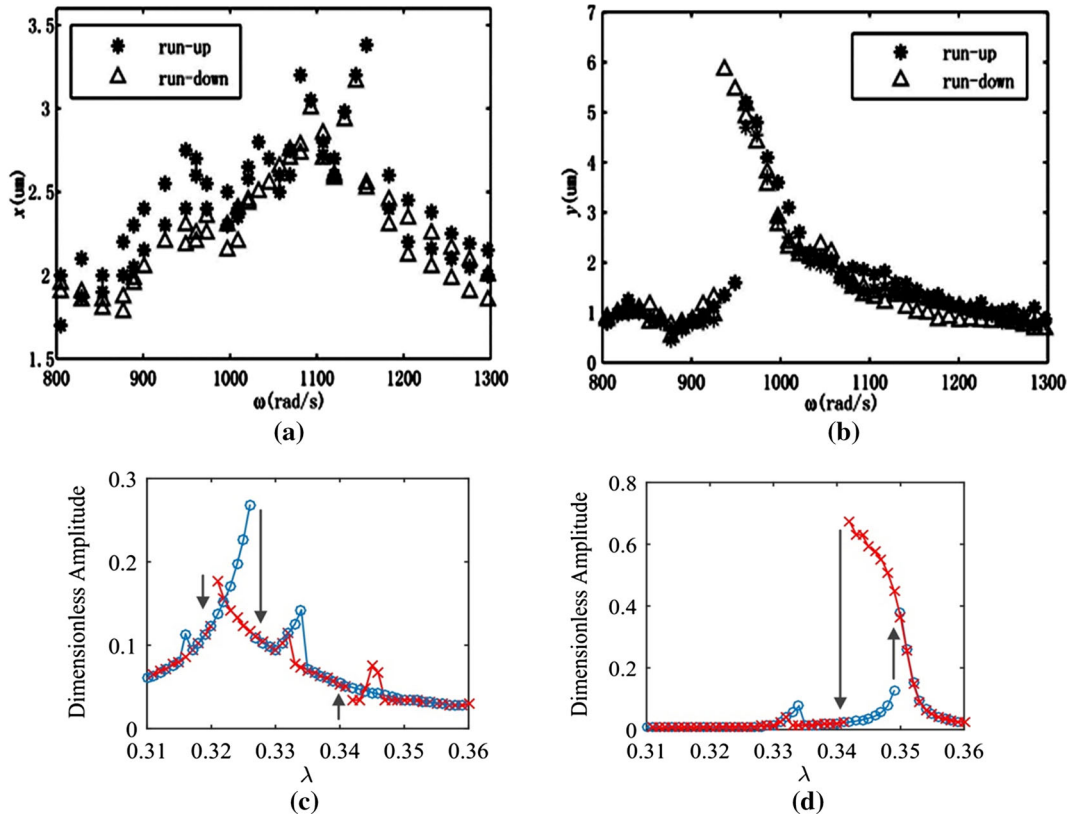


**Fig. 4** Comparison of numerical results of nonlinear characteristics at parametric resonance region with experiment results: **a** Coexistence of the soft and hard spring characteristic in experiment result [13]; **b** Soft spring characteristic in experiment result [13]; **c** Coexistence of the soft and hard spring characteristic in numerical result (where  $\circ$  indicates run-up, and  $\times$  indicates run-down); **d** Soft spring characteristic in numerical result (where  $\circ$  indicates run-up, and  $\times$  indicates run-down)

Figures 5 and 6 show the amplitude-frequency curves of the vibration of the disk center in the horizontal direction and the vertical direction in the VC frequency resonant region, respectively, when the number of balls varies from  $N_b = 8$  to  $N_b = 13$ .

When  $N_b = 8$ , the dimensionless VC frequency  $\omega_{vc} = 2.88$ . Because the horizontal and vertical natural frequencies are different, there are two resonance zones near  $\lambda_{v1x} = 0.326$  and  $\lambda_{v1y} = 0.351$ , respectively, which can be seen in Fig. 5a. The former one is a horizontal resonance region, and the latter is a horizontal-vertical coupled resonance region. Both of them have the jump hysteresis phenomenon. As mentioned before, a soft-hard spring characteristic is exhibited in the horizontal direction [22] (Fig. 5a). At where essentially saddle-node bifurcation occurs, however the intersection on the amplitude-frequency curve is not the exact bifurcation point, but a projection of the solution curve in the variable space [23]. This response characteristic indicates that there is a strong coupling between the two DOFs. In the vertical resonance region (Fig. 6a), the response exhibits a soft stiffness characteristic only, which means there is little coupling effect.

Although the soft stiffness characteristic dominates in vertical direction, it's also can be seen in Fig. 6a, there are multiple solutions and jumps around the point  $\lambda = 0.33$ . Take the data from run-up and run-down processes, the FFT (Fast Fourier Transform) analysis results (shown in Fig. 7a, b) show that in run-down process there is 2.88 frequency component (Fig. 7b), which corresponds to the VC frequency, and in run-up process, besides 2.88 frequency component, there is another 2.74 frequency component (Fig. 7a), which is not a periodic combination frequency of the unbalanced frequency and VC frequency. Thus, it is a quasi-periodic response. This phenomenon will be analyzed and discussed in detail later.

In addition, by the FFT analysis in the range of the horizontal-vertical coupling resonance region  $\lambda = 0.345$  (shown in Fig. 7c, d), it can be found that a quasi-periodic motion of the frequency  $\omega = 2.502$  in the run-down process appears (Fig. 7d), which causes the jump in the horizontal direction at corresponding point (Fig. 5a). While in run-up process, there is only a periodic motion (Fig. 7c).

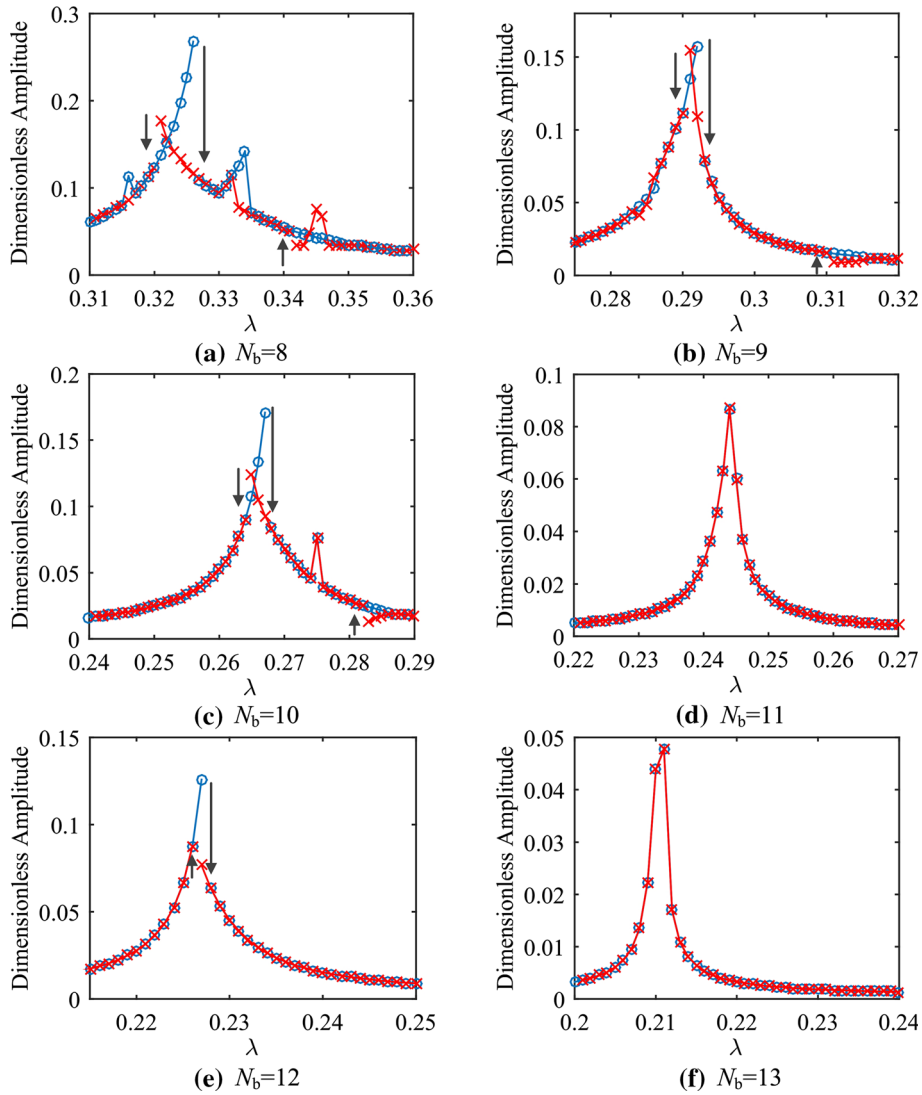


**Fig. 5** Amplitude-frequency curves along the horizontal direction (where  $\circ$  indicates run-up, and  $\times$  indicates run-down)

Going through Figs. 6 and 7, there are some other characteristics can be found. Compared with Fig. 5b–f, it can be seen that as the number of balls increases, the soft and hard spring coexistence characteristic in the horizontal direction generally weakens, and the resonance peak also decreases. However, this phenomenon is not monotonous, but varies according to parity of the  $N_b$ . In the case of  $N_b$  is an odd number, the amplitudes are larger, the nonlinear forces are stronger and the hysteresis zone is wider than those in the case that  $N_b$  is an even number.

Grouped by the parity of the  $N_b$ , the nonlinear characteristics of the system show the regularity of monotonous change in each group: (1) for the even group, as the number of balls increases, the system’s soft-hard spring coexistence characteristic gradually changes to hard spring characteristic. (2) For odd group, nonlinear characteristic disappears as the number of balls increases. In summary, the nonlinear characteristics would be weakened by the increase in the number of balls, but fluctuate regularly.

The trend in the vertical direction follows the same law. If  $N_b$  increases from an even number to an odd one, the amplitude decreases. On the contrary, the amplitude does not substantially change or increase a little. Meanwhile, as  $N_b$  increases, the amplitude in the vertical direction is gradually smaller than the amplitude in the horizontal direction, indicating that  $N_b$  has more influence on the stiffnesses of the system in vertical direction.



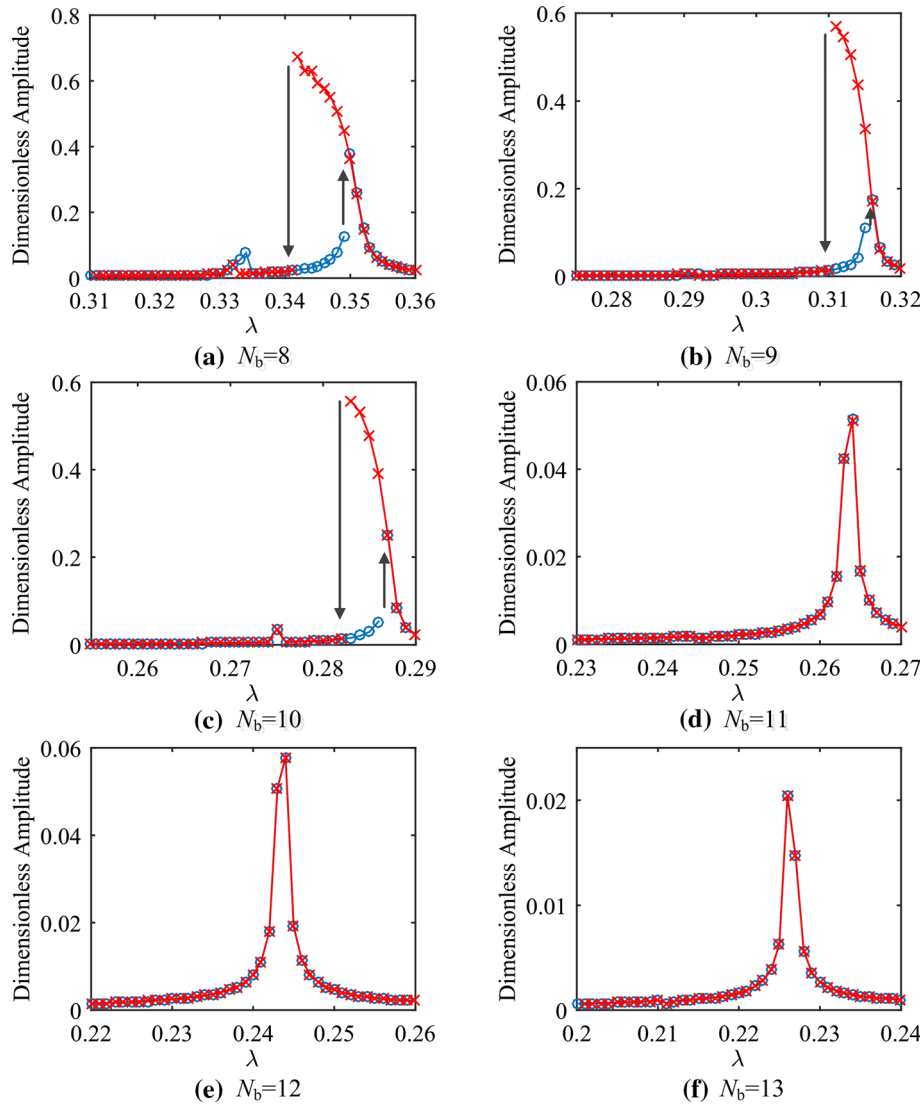


**Fig. 6** Amplitude-frequency curves along the vertical direction (where  $\circ$  indicates acceleration, and  $\times$  indicates deceleration)

### 3.3 The 1/2 sub-harmonic VC frequency resonance region

For the rolling bearing supported rotor system, as the strong nonlinear terms introduced by the bearing force, there exist not only base frequency responses, but also integer multiple or fractional harmonic responses, which could lead to resonance. When these harmonic responses are consistent with the natural frequencies of the system, the system resonance will be excited [19,20]. The 1/2 sub-harmonic resonance of the VC frequency will be studied in this section. When  $N_b = 8$ , the first VC resonance frequency of the system in the horizontal direction will be at  $\lambda = 0.326$ . So if there is a 1/2 sub-harmonic resonance of the VC frequency exists, it will be around  $\lambda = 0.652$ . Simulating around the point, as shown in Fig. 8a, a resonance peak appears in the horizontal direction. Taking point  $P_1(\lambda = 0.634)$ , at where the response is about to enter the peak, and point  $P_2(\lambda = 0.635)$ , at where the response has just started to increase, to conduct FFT analysis, the results are shown in Fig. 9a, b.

Figure 9a, b shows the frequency components of the system before and after entering the sub-harmonic resonance region, respectively. It is noting that the dominated frequency of the system response changes from the unbalanced excitation frequency (base frequency) to the 1/2 VC frequency. Before the resonant peak, the response component consists of the excitation frequency, VC frequency, and the combination of them, while the spectrum of the solutions on the peak shows the 1/2 sub-harmonic component of the parametric

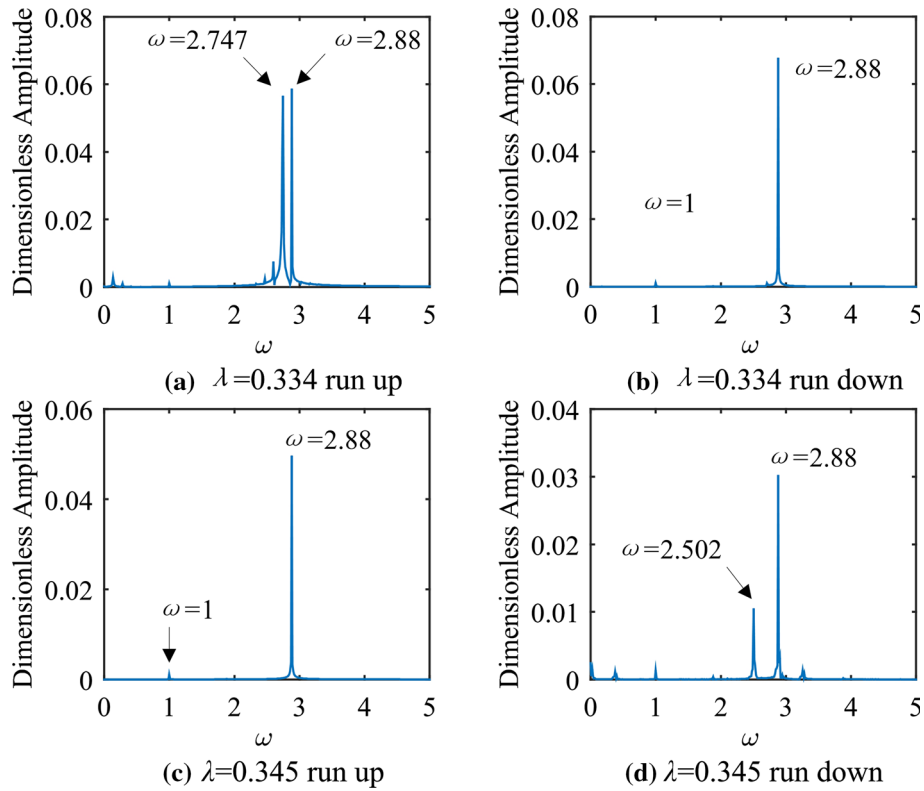


Fig. 7 Spectrum of response frequencies at VC frequency resonance region when  $N_b = 8$

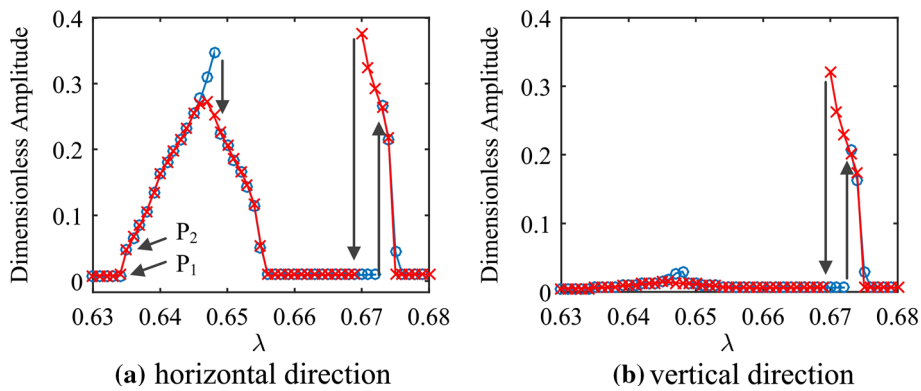


Fig. 8 Frequency–amplitude curves of the center of disk (where  $\circ$  indicates run-up, and  $\times$  indicates run-down)

frequency (VC frequency) dominants. This means that the system arises a period-doubling bifurcation under the influence of the VC frequency suddenly, which should be related to the parametric characteristic of the VC frequency. There is also a sudden jump at the sub-harmonic resonance peak. In run-up process, it jumps downward obviously, while in run-down process, it does not. This is a typical hard spring characteristic. In Fig. 8a, another resonant peak can be found around  $\lambda = 0.670$ . By the FFT analysis of run-up and run-down process around the point (shown in Fig. 9c, d), a quasi-period solution can be found.

Considering the effect of the number of ball  $N_b$ , the amplitude-frequency curves around the sub-harmonic VC frequency resonance region with different  $N_b$  are simulated, which are shown in Fig. 10a–e.

When  $N_b$  changes, the variation characteristic of the amplitude of 1/2 sub-harmonic VC frequency and the range of the resonance region also depends on the parity of  $N_b$ , as shown in Fig. 10a–e. When  $N_b$  is an odd number, the VC frequency sub-harmonic resonance region is smaller than the adjacent even number case. Similar to the case of the VC frequency resonance region, when  $N_b$  increases, generally, the resonance

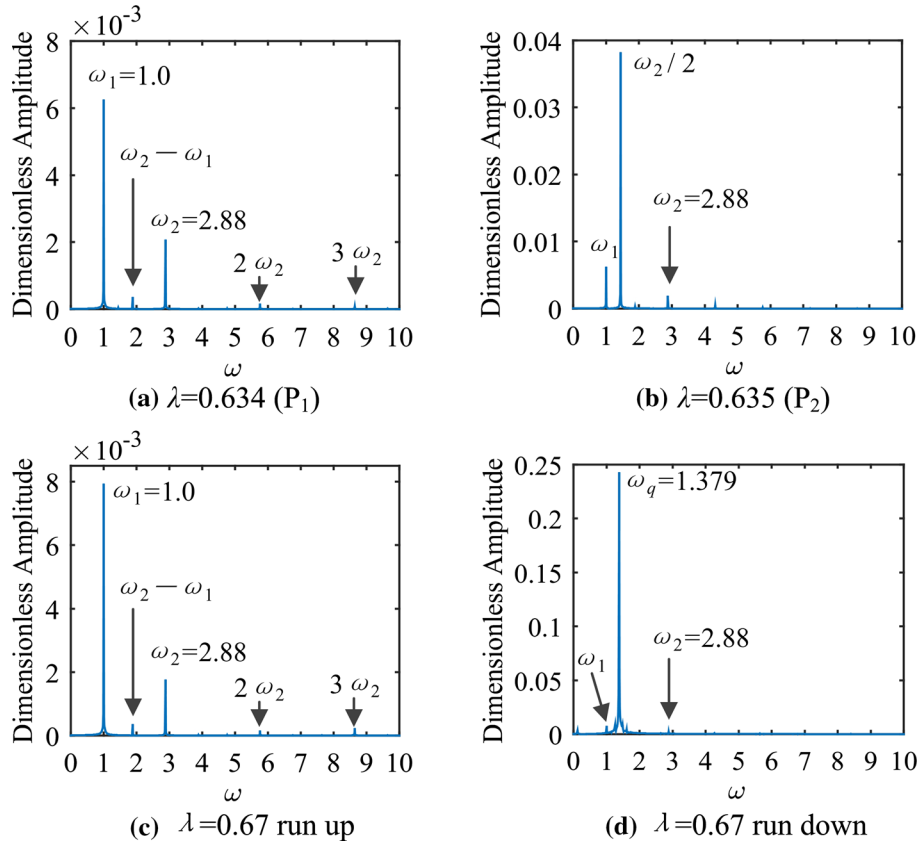


Fig. 9 Frequency components in sub-harmonic zone

region reduces and the amplitude decreases. In addition, even if the resonance peak is small, there is still a multi-solution phenomenon, which means strong bearing nonlinearity of the bearing support structure.

To the vertical direction, the analysis process is similar. But two points should be noticed. The first, as shown in Fig. 8b, because the VC frequency of the vertical direction is different from the horizontal direction, the sub-harmonic resonance won't appear simultaneously in both directions. The little peak in Fig. 8b around  $\lambda = 0.652$  is coupled by the response of horizontal direction, but the coupling effect is weak. The second, in some case, like when  $N_b = 7$ , there is no 1/2 sub-harmonic resonance as shown in Fig. 10f.

The reason should be that unlike the horizontal direction, the vertical direction is asymmetric in geometry due to the gravity. At the same time, the equivalent stiffness is greater than that of the horizontal direction. Both asymmetric and rigid factors may cause the conditions of sub-harmonic resonance to be different. When  $N_b = 7$ , the first-order vertical frequency is 298 rad/s. If sub-harmonic resonance occurs in the vertical direction, the resonance region should be near  $\lambda = 0.788$ . However, in Fig. 10f, there is no 1/2 sub-harmonic VC frequency resonance peak, which indicates that the stiffness is not the main factor affecting the vertical sub-harmonic VC frequency conditions. It should be the asymmetry caused by gravity that changes the conditions for the occurrence of sub-harmonic resonances in the vertical direction and inhibits its occurrence.

### 3.4 The quasi-periodic resonance region

According to the foregoing analysis, it can be seen that the system has quasi-periodic motion. Because the frequency of quasi-periodic response is not proportional to the unbalanced excitation frequency or VC frequency, it is hard to predict. In this section, we want to find some rules of quasi-periodic resonances.

When  $N_b = 8$ , the amplitude-frequency curve is simulated in a wide range after the first-order main resonance, which is shown in Fig. 11. Going through Fig. 11, it is noting that near  $\lambda = 5.96$  (the third-order natural frequency), a resonance band with a large span appears. By FFT analysis at  $\lambda = 5.94$ ,  $\lambda = 6.12$  and  $\lambda = 6.68$ , respectively, as shown in Fig. 12, it can be found that the system has obvious quasi-periodic

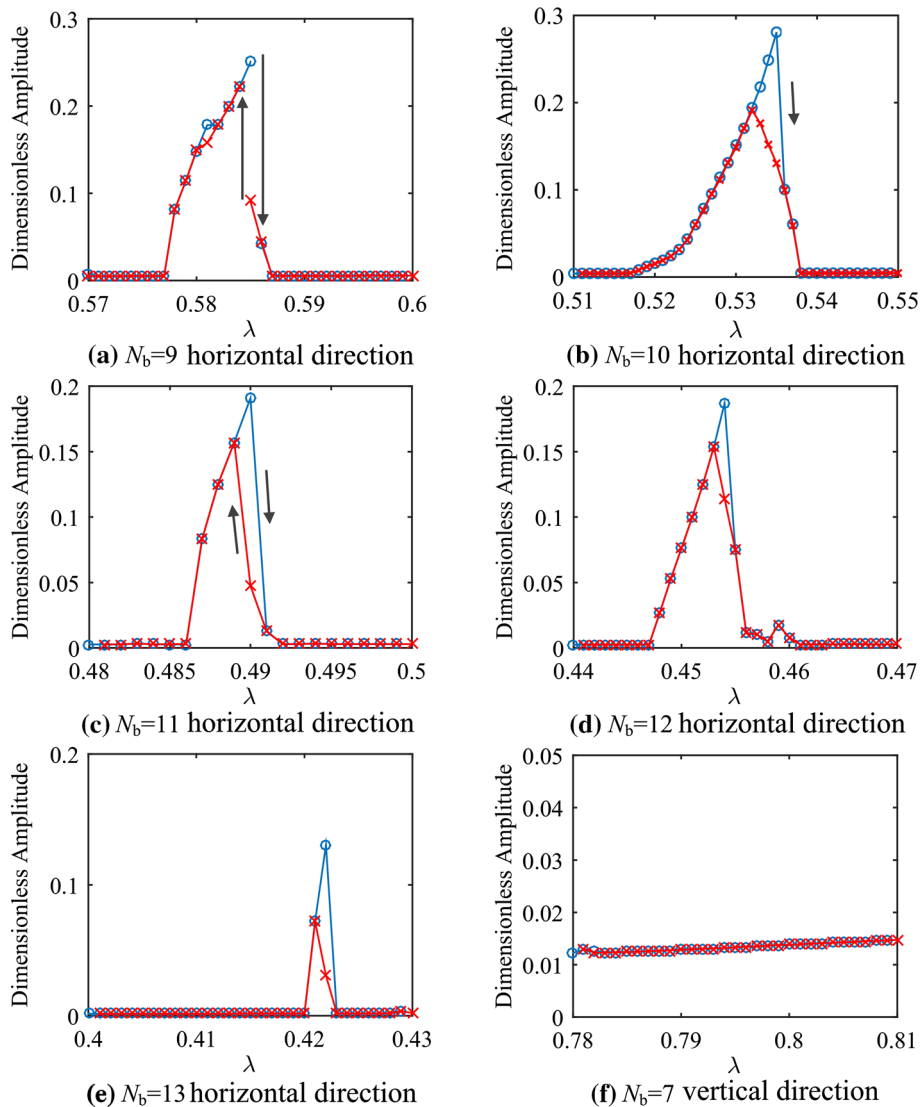


**Fig. 10** Frequency–amplitude curves at sub-harmonic resonance region with different numbers of rolling balls (where  $\circ$  indicates run-up, and  $\times$  indicates run-down)

frequency components, which amplitudes are greater than the periodic component. Thus, we can say, the quasi-periodic response is dominant.

Introducing a definition of an absolute quasi-periodic frequency  $\lambda_f = \lambda \cdot \omega$ , the quasi-periodic components in Fig. 12 can be calculated as (a) 0.943 and 2.683, (b) 0.971, and (c) 0.980. Compared with Fig. 3, the dominant quasi-periodic components locate on the first-order primary resonance region, while  $\lambda_f = 2.683$  corresponds to the second-order primary resonance region if you take further analysis. The reason is that the quasi-periodic motion can be formed by the secondary Hopf bifurcation of the periodic solution. Similar to the intrinsic property of the Hopf bifurcation excitation system, the second Hopf bifurcation can also excite the inherent properties of the system, i.e., the natural frequency of each order. Especially, the lower orders of resonance are easier to be excited, so the quasi-periodic motions are more likely to form in first-order primary resonance band. Unlike linear system, where resonance does not occur as long as it is far from the resonance region, the quasi-periodic response is a nonlinear characteristic, and could occur in the non-primary resonant region.

In Fig. 11, there are also some other quasi-periodic motions need to be noticed in the range of  $\lambda = 2.0$  and  $\lambda = 4.0$ . Taken the FFT analysis results of  $\lambda = 2.2$ ,  $\lambda = 2.76$ , and  $\lambda = 3.08$  (shown in Fig. 13), the absolute quasi-periodic components frequency are (a) 0.860, (b) 0.943, 5.862, and (c) 0.940, which correspond to the first-order and third-order primary resonance regions of the system, respectively. It can be seen that in these

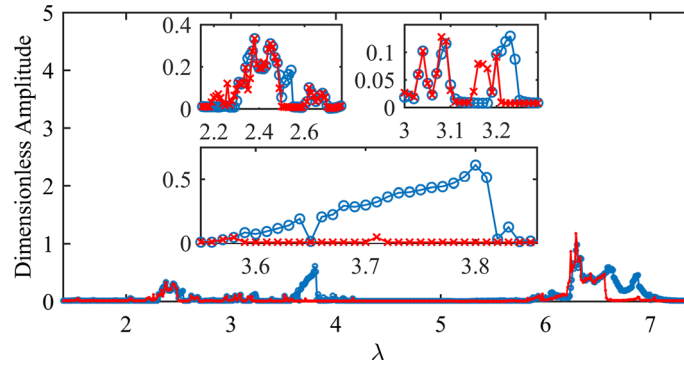


**Fig. 11** Frequency–amplitude curve of horizontal direction when  $N_b = 8$  (where  $\circ$  indicates run-up, and  $\times$  indicates run-down)

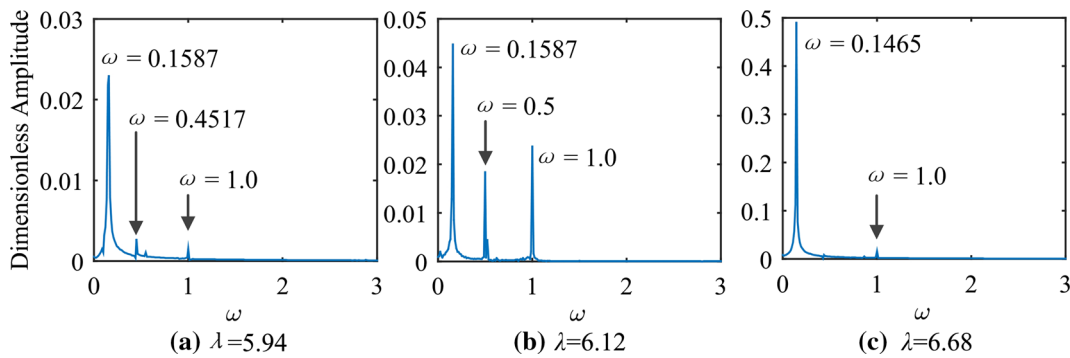


**Fig. 12** Frequency spectrum at third primary resonance region

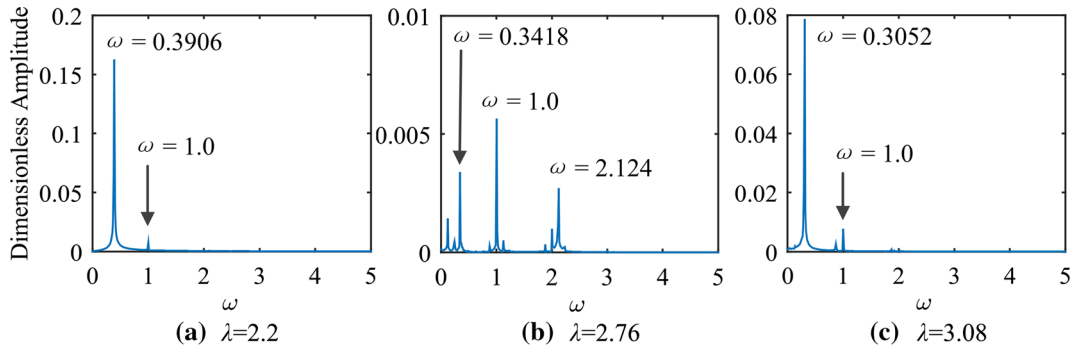


**Fig. 13** Frequency spectrum when  $N_b = 8$

frequency intervals, the system has non-coordinated responses concentrated, and each quasi-periodic solution is connected into a complex motion region.

In the range of  $\lambda = 3.6$  to  $\lambda = 3.8$ , it is noted that the amplitudes are different in run-up and run-down processes. Along run-up curve, the amplitude gradually increases until it jumps to a lower amplitude value, while in the case of run-down, the amplitude keeps a low value. Taking the FFT analysis (shown in Fig. 14), the increment of the amplitude is derived from the quasi-periodic motion with the frequency 0.923, which locates in the first-order resonance region (main resonance), and has same trend as that of the main resonance region. Comparing the frequency components in run-up and run-down cases, there is a combination of the quasi-periodic frequency and the excitation frequency exhibits in run-up case, while, there is no quasi-periodic motion in run-down case, and only the external excitation frequency component exists. Therefore, in this interval, the system is characterized by the coexistence of the periodic solution and the quasi-periodic solution, which is a kind of bi-stable characteristic.

When the number of balls  $N_b = 9$ , the amplitude-frequency curve in the horizontal direction of the disk center is shown in Fig. 15. Compared with the case of  $N_b = 8$ , although there are similar multiple peaks,

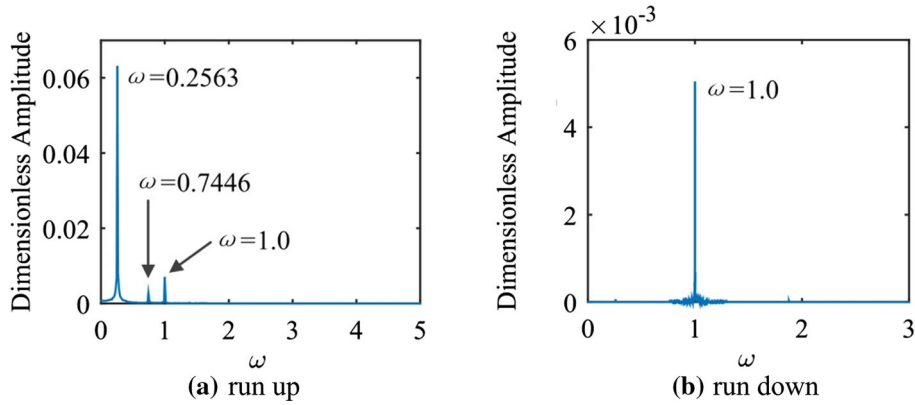


Fig. 14 Frequency spectrum, when  $N_b = 8$  at  $\lambda = 3.6$

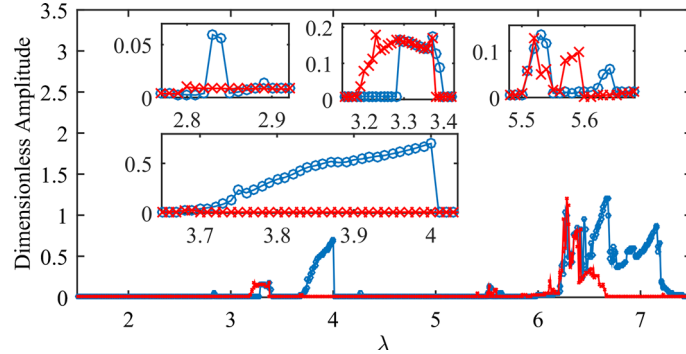


Fig. 15 Frequency–amplitude curve of horizontal direction (where  $\circ$  indicates run-up, and  $\times$  indicates run-down)

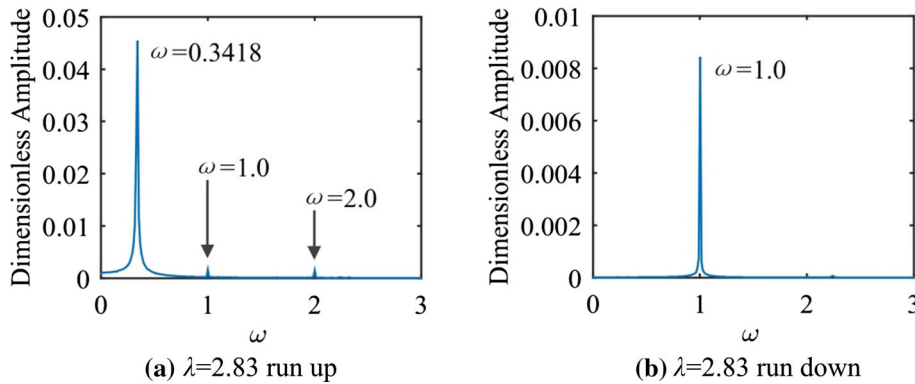


Fig. 16 Frequency spectrum in second primary resonance region when  $N_b = 9$

all the resonance regions are relatively independent and no connected regions like interval  $\lambda = 2.0$  to  $4.0$  in Fig. 11 form.

Meanwhile, we notice that in the interval of  $\lambda = 2.8$  to  $2.9$ , the amplitude of the horizontal direction is relatively small, but the coexistence characteristic emerges. As there are quasi-periodic frequency and superharmonic components in run-up process, while there is only periodic component in the run-down process, which are shown in Fig. 16a, b. In addition, there are multiple regions in which periodic solutions and quasi-periodic solutions coexist, such as  $\lambda = 3.2 \sim 3.3$ ,  $\lambda = 3.7 \sim 4.0$  and  $\lambda = 5.55 \sim 5.65$ . The spectrum of quasi-periodic solutions and periodic solutions are shown in Fig. 17, and the frequencies corresponding to the quasi-periodic solution are  $\lambda_f = 0.931$ ,  $\lambda_f = 0.947$ , and  $\lambda_f = 0.955$ .

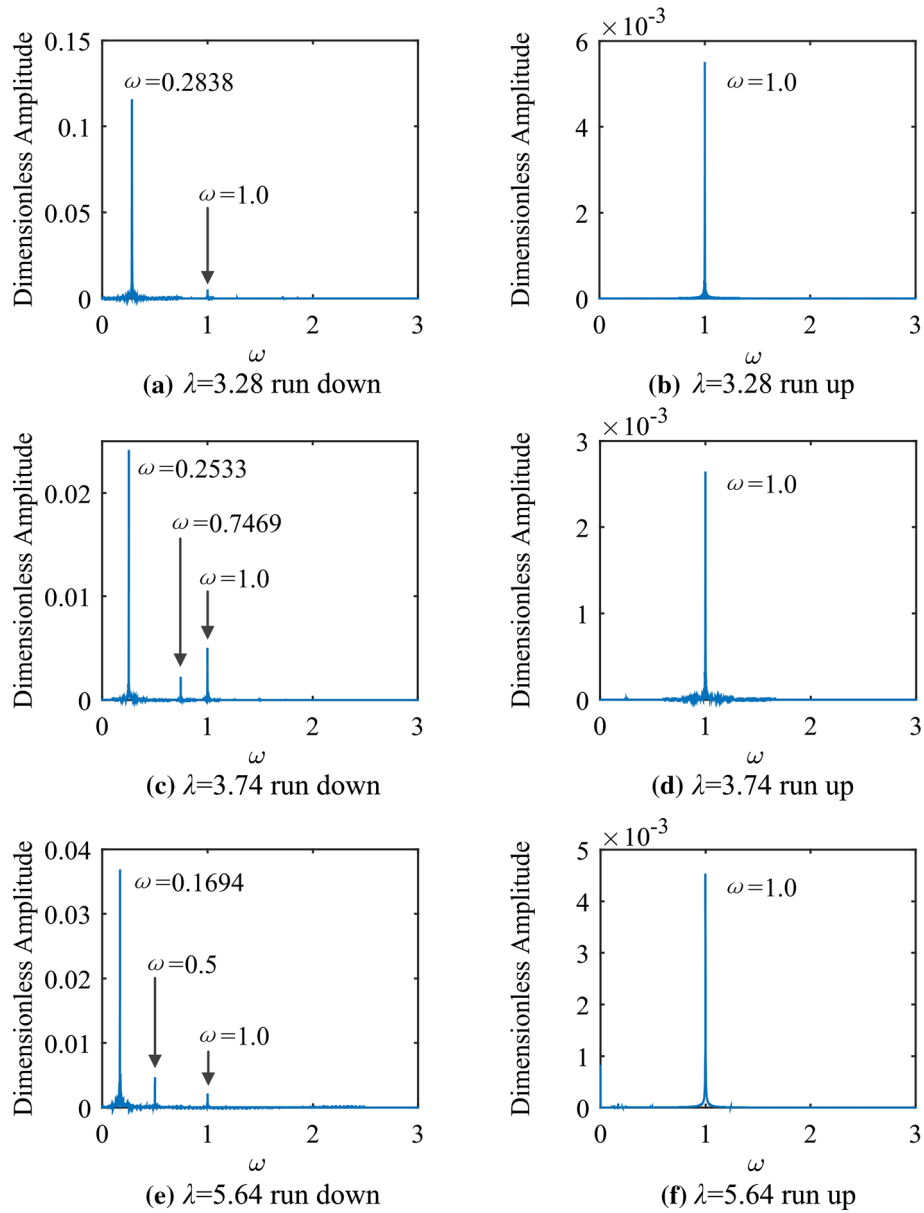


Fig. 17 Frequency spectrum when  $N_b = 9$

In the third-order resonance region ( $\lambda = 6$  to  $7.5$ ), there still exists a series of quasi-periodic responses. The corresponding frequencies are listed in Table 3, which all meet the rule of that both of them locate in the first-order primary resonance region.

In order to analyze the effects of the number of balls, Fig. 18 shows amplitude-frequency curves in the horizontal direction when the number of balls are  $N_b = 10$ ,  $N_b = 11$ ,  $N_b = 12$ , and  $N_b = 13$ , respectively. And the quasi-periodic frequencies corresponding to each ball number are shown in Table 4. As the number of balls increases, most of the quasi-periodic areas in the system show a decreasing trend. Noting that  $\lambda = 2.4$  at  $N_b = 8$  (Fig. 11),  $\lambda = 1.95$  at  $N_b = 10$  (Fig. 18a),  $\lambda = 1.61$  at  $N_b = 12$  (Fig. 18c), there are quasi-periodic motions, whose frequencies are  $\lambda_f = 0.9228$ ,  $\lambda_f = 0.9522$ , and  $\lambda_f = 0.9827$ .

Multiplied by the corresponding VC frequencies of 2.88, 3.6, and 4.32, it can be found that the multiple results 6.912, 7.02, and 6.955 locate in the third-order natural resonance region. Therefore, it can be seen that these three resonance points are approximately the VC frequency resonance points in third-order natural resonance region. These frequencies connect the low-order resonance regions and high-order resonance regions.

**Table 3** Quasi-period frequencies at third primary resonance region

| $\lambda$ | $\omega$ | $\lambda_f$ |
|-----------|----------|-------------|
| 6.28      | 0.1587   | 0.9966      |
| 6.45      | 0.1536   | 0.9907      |
| 6.66      | 0.1465   | 0.9757      |
| 7.16      | 0.1404   | 1.0053      |

**Table 4** Quasi-period frequencies at others region

| $N_b$ | $\lambda$ | $\omega$ | $\lambda_f$ |
|-------|-----------|----------|-------------|
| 10    | 3.4       | 0.2808   | 0.9547      |
| 10    | 3.8       | 0.2518   | 0.9568      |
| 10    | 5.15      | 0.1862   | 0.9589      |
| 11    | 3.38      | 0.2869   | 0.9697      |
| 11    | 3.5       | 0.2747   | 0.9614      |
| 11    | 4.0       | 0.2441   | 0.9764      |
| 12    | 3.43      | 0.2808   | 0.9631      |
| 12    | 4.01      | 0.2441   | 0.9788      |
| 12    | 4.65      | 0.2075   | 0.9648      |
| 13    | 4.08      | 0.2441   | 0.9959      |

However, when the number of balls is odd, no such phenomenon occurs, which also shows that the system with odd number of balls is more stable.

It can be known from the above analysis that most of the quasi-periodic frequencies of the system are concentrated at the first-order resonance peak, and the quasi-periodic motion is more likely to occur due to the wider resonance band of the nonlinear system. In addition, some quasi-periodic regions do not show obvious regularity. Increasing the number of balls can only reduce the amplitude of some quasi-periodic solutions, but the effects are not obvious for a wide range of quasi-periodic solutions. The quasi-periodic motion is a non-harmonic response of the system that generates a natural vibration frequency in the non-resonant region. Its amplitude is directly related to the low-order peak. Therefore, the suppression of the quasi-periodic vibration should be considered in terms of suppressing the main peak. Controlling the low-order resonance peak can reduce the maximum amplitude of the vibration on the one hand and suppress the generation of related quasi-periodic motions on the other.

#### 4 Conclusion remarks

This paper studies the nonlinear response characteristics of an asymmetric rolling bearing-rotor system in multiple resonance regions, and draws the following conclusions.

- (1) Due to the effect of the VC frequency of the bearing, the system has VC frequency resonance regions corresponding to the main resonance regions. In the horizontal direction, there is a nonlinear characteristic of the coexistence of soft-hard stiffness, and in the vertical direction, only soft stiffness exists. This means the vertical direction affects the horizontal direction much, on the contrary, there is almost no effect.
- (2) Due to the asymmetry and nonlinearity, there is a sub-harmonic resonance of the VC frequency in the horizontal direction, which has hard spring characteristic, while there is no sub-harmonic resonance of the VC frequency in the vertical direction.
- (3) There are many quasi-periodic motions in the system, the frequencies of which are distributed at the natural resonance region of each order of the system, especially concentrate in the first-order main resonance region. There is a close relationship between the first-order main resonance and the quasi-periodic motions.
- (4) The increase in the number of balls increases the stiffness of the system's supports, thereby it will reduce the amplitude and suppress the nonlinear behaviors of the system. But there are fluctuations in amplitude and resonances in the VC frequency resonance regions and its 1/2 sub-harmonic resonance regions. Among them, the resonance peak values in the resonance interval of the odd-numbered balls are smaller than those of the adjacent even-numbered balls.



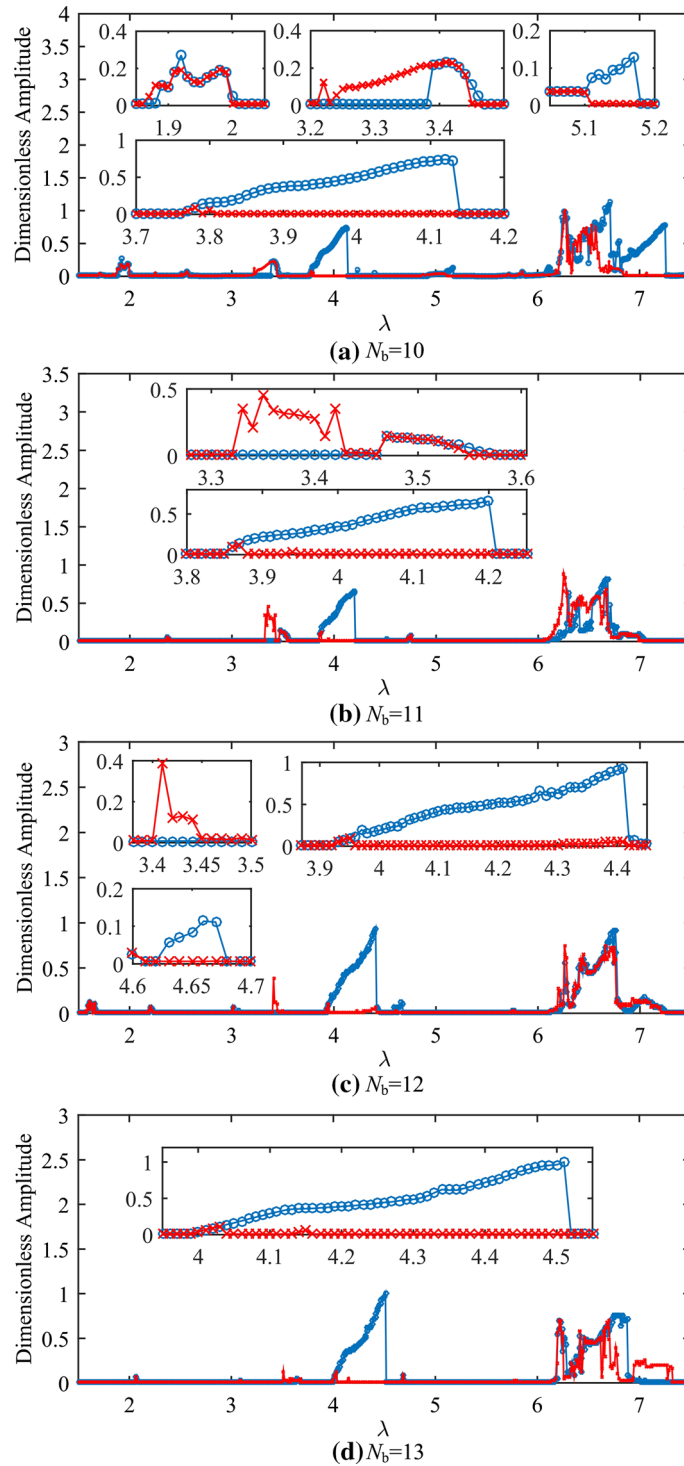


**Fig. 18** Amplitude-frequency curves along the longitude direction of the disk center (where  $\circ$  indicates acceleration,  $\times$  indicates deceleration,  $N_b = 10$ )

All these characteristics can help us understand the dynamic behaviors of the ball bearing-rotor systems and because they are all present in a healthy bearing condition and therefore can be used to establish base-line behavior as a function of system parameters.

In the study, the frequency prediction of the occurrence of the quasi-periodic and the occurrence conditions of the frequency 1/2 sub-harmonics are worthy of further systematic research. In the future, further analysis will be conducted related to these two points.

**Acknowledgements** This work was supported by Shandong Provincial Natural Science Foundation, China (Grant Nos. ZR2018BA021 and ZR2018QA005 ), the China Postdoctoral Science Foundation (Grant No. 2017M622259), and the National Natural Science Foundation of China (Grant Nos. 11502161, 11902184).

**Declarations**

**Conflict of interest** On behalf of all authors, the corresponding author states that there is no conflict of interest.

**A Appendix**

Expanded form of Eq. (1)

$$\begin{cases} m\ddot{x} + c_1(\dot{x} - \dot{x}_1) - c_2(\dot{\theta}_y - \dot{\theta}_{y1}) + k_{rr}(x - x_1) - k_{r\varphi}(\theta_y - \theta_{y1}) = m\delta\Omega^2 \cos \Omega t \\ m\ddot{y} + c_1(\dot{y} - \dot{y}_1) + c_2(\dot{\theta}_x - \dot{\theta}_{x1}) + k_{rr}(y - y_1) + k_{r\varphi}(\theta_x - \theta_{x1}) = m\delta\Omega^2 \sin \Omega t - mg \\ J_d\ddot{\theta}_x + J_p\Omega\dot{\theta}_y + c_3(\dot{y} - \dot{y}_1) + c_4(\dot{\theta}_x - \dot{\theta}_{x1}) + k_{\varphi r}(y - y_1) + k_{\varphi\varphi}(\theta_x - \theta_{x1}) = 0 \\ J_d\ddot{\theta}_y - J_p\Omega\dot{\theta}_x - c_3(\dot{x} - \dot{x}_1) + c_4(\dot{\theta}_y - \dot{\theta}_{y1}) - k_{\varphi r}(x - x_1) + k_{\varphi\varphi}(\theta_y - \theta_{y1}) = 0 \\ m_a\ddot{x}_a - \gamma_2c_1(\dot{x} - \dot{x}_1) + \gamma_2c_2(\dot{\theta}_y - \dot{\theta}_{y1}) - \gamma_2k_{rr}(x - x_1) + \gamma_2k_{r\varphi}(\theta_y - \theta_{y1}) + F_{bx1} = 0 \\ m_a\ddot{y}_a - \gamma_2c_1(\dot{y} - \dot{y}_1) - \gamma_2c_2(\dot{\theta}_x - \dot{\theta}_{x1}) - \gamma_2k_{rr}(y - y_1) - \gamma_2k_{r\varphi}(\theta_x - \theta_{x1}) + F_{by1} = -m_ag \\ m_b\ddot{x}_b - \gamma_1c_1(\dot{x} - \dot{x}_1) + \gamma_1c_2(\dot{\theta}_y - \dot{\theta}_{y1}) - \gamma_1k_{rr}(x - x_1) + \gamma_1k_{r\varphi}(\theta_y - \theta_{y1}) + F_{bx2} = 0 \\ m_b\ddot{y}_b - \gamma_1c_1(\dot{y} - \dot{y}_1) - \gamma_1c_2(\dot{\theta}_x - \dot{\theta}_{x1}) - \gamma_1k_{rr}(y - y_1) - \gamma_1k_{r\varphi}(\theta_x - \theta_{x1}) + F_{by2} = -m_bg \\ m_o\ddot{x}_o + k_ax_o - F_{bx2} = 0 \\ m_o\ddot{y}_o + k_ay_o - F_{by2} = -m_og \end{cases}$$

where  $x_1 = \gamma_2x_a + \gamma_1x_b$ ,  $y_1 = \gamma_2y_a + \gamma_1y_b$ ,  $\theta_{x1} = (y_b - y_a)/l$  and  $\theta_{y1} = (x_a - x_b)/l$  represent the disk center’s rigid body displacements and rotation angles, respectively;  $l = l_1 + l_2$  is the total length of the rotating shaft;  $l_1$  is the length of left part of the shaft, while  $l_2$  is the right;  $m$ ,  $m_a$ ,  $m_b$  and  $m_o$  represent the equivalent mass of the hub, the left and right journals and the outer ring of the bearing, respectively;  $k_{rr}$ ,  $k_{r\varphi}$ ,  $k_{\varphi r}$  and  $k_{\varphi\varphi}$  represent the equivalent stiffness of the shaft in different directions, respectively;  $J_d$  and  $J_p$  represent the moment of inertia and pole moment of inertia of the wheel equator, respectively;  $c_1 - c_4$  represent the equivalent damping coefficients of the rotating shaft;  $\gamma_1$  and  $\gamma_2$  are the length proportional coefficients, respectively, in which  $\gamma_1 = l_1/l$  and  $\gamma_2 = l_2/l$ ;  $\delta$  represents the eccentricity of the unbalanced mass;  $F_{bx1}$  and  $F_{by1}$  are the horizontal and vertical bearing forces at the left end, respectively;  $F_{bx2}$  and  $F_{by2}$  are the horizontal and vertical bearing force at the right end, respectively;  $g$  is the gravitational acceleration.

Expanded form of Eq. (5)

$$\begin{cases} q_1'' + \zeta_1q_1' - \zeta_2q_4' - (\zeta_2 + \zeta_1\gamma_2)q_5' + (\zeta_2 - \gamma_1\zeta_1)q_7' + \kappa_1q_1 - \kappa_2q_4 \\ -(\kappa_2 + \kappa_1\gamma_2)q_5 + (\kappa_2 - \gamma_1\kappa_1)q_7 = U_1 \cos \tau \\ q_2'' + \zeta_1q_2' - \zeta_2q_3' - (\zeta_2 + \zeta_1\gamma_2)q_6' + (\zeta_2 - \gamma_1\zeta_1)q_8' + \kappa_1q_2 - \kappa_2q_3 \\ -(\kappa_2 + \kappa_1\gamma_2)q_6 + (\kappa_2 - \gamma_1\kappa_1)q_8 = U_1 \sin \tau - W \\ \alpha_0q_3'' + \alpha_0\eta q_4' + \zeta_3q_2' + \zeta_4q_3' - (\zeta_4 + \zeta_3\gamma_2)q_6' + (\zeta_4 - \gamma_1\zeta_3)q_8' + \kappa_3q_2 + \kappa_4q_3 \\ -(\kappa_4 + \kappa_3\gamma_2)q_6 + (\kappa_4 - \gamma_1\kappa_3)q_8 = 0 \\ \alpha_0q_4'' - \alpha_0\eta q_3' - \zeta_3q_1' + \zeta_4q_4' + (\zeta_4 + \zeta_3\gamma_2)q_5' - (\zeta_4 - \gamma_1\zeta_3)q_7' - \kappa_3q_1 + \kappa_4q_4 \\ +(\kappa_4 + \kappa_3\gamma_2)q_5 - (\kappa_4 - \gamma_1\kappa_3)q_7 = 0 \\ \alpha_1q_5'' - \gamma_2\zeta_1q_1' + \gamma_2\zeta_2q_4' + \gamma_2(\zeta_2 + \gamma_2\zeta_1)q_5' - \gamma_2(\zeta_2 - \gamma_1\zeta_1)q_7' - \gamma_2\kappa_1q_1 + \gamma_2\kappa_2q_4 \\ +\gamma_2(\kappa_2 + \gamma_2\kappa_1)q_5 - \gamma_2(\kappa_2 - \gamma_1\kappa_1)q_7 + \bar{C}_b\bar{F}_{bx1} = 0 \\ \alpha_1q_6'' - \gamma_2\zeta_1q_2' - \gamma_2\zeta_2q_3' + \gamma_2(\zeta_2 + \gamma_2\zeta_1)q_6' - \gamma_2(\zeta_2 - \gamma_1\zeta_1)q_8' - \gamma_2\kappa_1q_2 - \gamma_2\kappa_2q_3 \\ +\gamma_2(\kappa_2 + \gamma_2\kappa_1)q_6 - \gamma_2(\kappa_2 - \gamma_1\kappa_1)q_8 + \bar{C}_b\bar{F}_{by1} = -\alpha_1W \\ \alpha_2q_7'' - \gamma_1\zeta_1q_1' + \gamma_1\zeta_2q_4' + \gamma_1(\zeta_2 + \gamma_2\zeta_1)q_5' - \gamma_1(\zeta_2 - \gamma_1\zeta_1)q_7' - \gamma_1\kappa_1q_1 + \gamma_1\kappa_2q_4 \\ +\gamma_1(\kappa_2 + \gamma_2\kappa_1)q_5 - \gamma_1(\kappa_2 - \gamma_1\kappa_1)q_7 + \bar{C}_b\bar{F}_{bx2} = 0 \\ \alpha_2q_8'' - \gamma_1\zeta_1q_2' - \gamma_1\zeta_2q_3' + \gamma_1(\zeta_2 + \gamma_2\zeta_1)q_6' - \gamma_1(\zeta_2 - \gamma_1\zeta_1)q_8' - \gamma_1\kappa_1q_2 - \gamma_1\kappa_2q_3 \\ +\gamma_1(\kappa_2 + \gamma_2\kappa_1)q_6 - \gamma_1(\kappa_2 - \gamma_1\kappa_1)q_8 + \bar{C}_b\bar{F}_{by2} = -\alpha_2W \end{cases}$$

$$\begin{cases} \alpha_3 q_9'' + \kappa_5 q_9 - \bar{C}_b \bar{F}_{bx1} = 0 \\ \alpha_3 q_{10}'' + \kappa_5 q_{10} - \bar{C}_b \bar{F}_{by1} = -\alpha_2 W \end{cases}$$

where  $q_1 = x/c$ ,  $q_2 = y/c$ ,  $q_3 = \theta_x l/c$ ,  $q_4 = \theta_y l/c$ ,  $q_5 = x_a/c$ ,  $q_6 = y_a/c$ ,  $q_7 = x_b/c$ ,  $q_8 = y_b/c$ ,  $q_9 = x_o/c$  and  $q_{10} = y_o/c$  are dimensionless displacements of the disk center, the left and right journals, and the outer ring. The dimensionless forces  $\bar{F}_{bx1}$ ,  $\bar{F}_{bx2}$ ,  $\bar{F}_{by1}$ , and  $\bar{F}_{by2}$  have same expressions as shown in Eqs. (3) and (4), respectively, just with the replacement of the corresponding dimensionless parameters.

All other dimensionless parameters are listed as  $\alpha_0 = J_d/ml^2$ ,  $\alpha_1 = m_a/m$ ,  $\alpha_2 = m_b/m$ ,  $\alpha_3 = m_o/m$ ,  $\kappa_1 = k_{rr}/m\Omega^2$ ,  $\kappa_2 = k_{r\varphi}/ml\Omega^2$ ,  $\kappa_3 = k_{\varphi r}/ml\Omega^2$ ,  $\kappa_4 = k_{\varphi\varphi}/ml^2\Omega^2$ ,  $\kappa_5 = k_a/m\Omega^2$ ,  $\zeta_1 = c_1/m\Omega$ ,  $\zeta_2 = c_2/ml\Omega$ ,  $\zeta_3 = c_3/ml\Omega$ ,  $\zeta_4 = c_4/ml^2\Omega$ ,  $\eta = J_p/J_d$ ,  $U_1 = \delta_1/c$ ,  $\bar{C}_b = C_b c^{0.5}/m\Omega^2$ , and  $W = g/c\Omega^2$ , in which  $c = mg/k$ .

## References

1. Fukata, S., Gad, E.H., Kondou, T., Ayabe, T., Tamura, H.: On the radial vibration of ball bearings: computer simulation. *Bull. JSME* **28**(239), 899–904 (1985)
2. Mevel, B., Guyader, J.L.: Routes to chaos in ball bearings. *J. Sound Vib.* **162**(3), 471–87 (1993)
3. Mevel, B., Guyader, J.L.: Experiments on routes to chaos in ball bearings. *J. Sound Vib.* **318**(3), 549–64 (2008)
4. Saito, S.: Calculation of nonlinear unbalance response of horizontal Jeffcott rotors supported by ball bearings with radial clearances. *J. Vib. Acoust.* **107**(4), 416–420 (1985)
5. Feng, N.S., Hahn, E.J.: Rolling element bearing non-linearity effects. In: *Turbo Expo: Power for Land, Sea, and Air*, vol. 78576, p. V004T03A034. American Society of Mechanical Engineers (2000)
6. Tiwari, M., Gupta, K., Prakash, O.: Dynamic response of an unbalanced rotor supported on ball bearings. *J. Sound Vib.* **238**(5), 757–79 (2000)
7. Tiwari, M., Gupta, K., Prakash, O.: Effect of radial internal clearance of a ball bearing on the dynamics of a balanced horizontal rotor. *J. Sound Vib.* **238**(5), 723–56 (2000)
8. Bai, C.Q., Xu, Q.Y., Zhang, X.L.: Nonlinear stability of balanced rotor due to effect of ball bearing internal clearance. *Appl. Math. Mech.* **27**(2), 175–86 (2006)
9. Kostek, R.: Analysis of the primary and superharmonic contact resonances—Part 1. *J. Theor. Appl. Mech.* **51**(2), 475–486 (2013)
10. Harsha, S.P., Sandeep, K., Prakash, R.: The effect of speed of balanced rotor on nonlinear vibrations associated with ball bearings. *Int. J. Mech. Sci.* **45**(4), 725–40 (2003)
11. Harsha, S.P.: Nonlinear dynamic response of a balanced rotor supported by rolling element bearings due to radial internal clearance effect. *Mech. Mach. Theory* **41**(6), 688–706 (2006)
12. Gupta, T.C., Gupta, K., Sehgal, D.K.: Nonlinear vibration analysis of an unbalanced flexible rotor supported by ball bearings with radial internal clearance. In: *Turbo Expo: Power for Land, Sea, and Air*, vol. 43154, pp. 1289–1298 (2008)
13. Jin, Y., Yang, R., Hou, L., Chen, Y., Zhang, Z.: Experiments and numerical results for varying compliance contact resonance in a rigid rotor-ball bearing system. *J. Tribol.* **139**(4), 041103 (2017)
14. Villa, C., Sinou, J.J., Thouverez, F.: Stability and vibration analysis of a complex flexible rotor bearing system. *Commun. Nonlinear Sci. Numer. Simul.* **13**(4), 804–21 (2008)
15. Maraini, D., Nataraj, C.: Nonlinear analysis of a rotor-bearing system using describing functions. *J. Sound Vib.* **420**, 227–41 (2018)
16. Yang, Y.F., Wu, Q.Y., Wang, Y.L., Qin, W.Y., Lu, K.: Dynamic characteristics of cracked uncertain hollow-shaft. *Mech. Syst. Signal Process.* **124**, 36–48 (2019)
17. Sinou, J.J.: Non-linear dynamics and contacts of an unbalanced flexible rotor supported on ball bearings. *Mech. Mach. Theory* **44**(9), 1713–32 (2009)
18. Zhang, Z., Chen, Y., Cao, Q.: Bifurcations and hysteresis of varying compliance vibrations in the primary parametric resonance for a ball bearing. *J. Sound Vib.* **350**, 171–84 (2015)
19. Harsha, S.P., Sandeep, K., Prakash, R.: Effects of preload and number of balls on nonlinear dynamic behavior of ball bearing system. *Int. J. Nonlinear Sci. Numer. Simul.* **4**(3), 265–78 (2003)
20. Aktürk, N., Uneeb, M., Gohar, R.: The effects of number of balls and preload on vibrations associated with ball bearings. *J. Tribol.* **119**(4), 747–753 (1997)
21. Hou, L., Chen, Y.S., Cao, Q.J., Zhang, Z.Y.: Turning maneuver caused response in an aircraft rotor-ball bearing system. *Nonlinear Dyn.* **79**(1), 229–240 (2015)
22. Zhang, Z.Y., Chen, Y.S., Li, Z.G.: Influencing factors of the dynamic hysteresis in varying compliance vibrations of a ball bearing. *Sci. China Technol. Sci.* **58**(5), 775–782 (2015)
23. Chen, H.Z., Hou, L., Chen, Y.S.: Bifurcation analysis of a rigid-rotor squeeze film damper system with unsymmetrical stiffness supports. *Arch. Appl. Mech.* **87**(8), 1347–1364 (2017)